# Computer Simulation of Intraventricular Flow and Pressure Gradients During Diastole

**J. A. Vierendeels**

**K. Riemslagh**

**E. Dick**
Mem. ASME

Department of Flow,
Heat, and Combustion Mechanics,
Institute Biomedical Technology,
Ghent University,
St.-Pietersnieuwstraat 41,
9000 Ghent, Belgium

**P. R. Verdonck**
Hydraulics Laboratory,
Institute Biomedical Technology,
Ghent University,
St.-Pietersnieuwstraat 41,
9000 Ghent, Belgium

*A two-dimensional axisymmetric computer model is developed for the simulation of the filling flow in the left ventricle (LV). The computed results show that vortices are formed during the acceleration phases of the filling waves. During the deceleration phases these are amplified and convected into the ventricle. The ratio of the maximal blood velocity at the mitral valve (peak E velocity) to the flow wave propagation velocity (WPV) of the filling wave is larger than 1. This hemodynamic behavior is also observed in experiments in vitro (Steen and Steen, 1994, Cardiovasc. Res., **28**, pp. 1821–1827) and in measurements in vivo with color M-mode Doppler echocardiography (Stugaard et al., 1994, J. Am. Coll. Cardiol., **24**, 663–670). Computed intraventricular pressure profiles are similar to observed profiles in a dog heart (Courtois et al., 1988, Circulation, **78**, pp. 661–671). The long-term goal of the computer model is to study the predictive value of noninvasive parameters (e.g., velocities measured with Doppler echocardiography) on invasive parameters (e.g., pressures, stiffness of cardiac wall, time constant of relaxation). Here, we show that higher LV stiffness results in a smaller WPV for a given peak E velocity. This result may indicate an inverse relationship between WPV and LV stiffness, suggesting that WPV may be an important noninvasive index to assess LV diastolic stiffness, LV diastolic pressure and thus atrial pressure (preload).*
[S0148-0731(00)01606-X]

## Introduction

Intraventricular pressure gradients during relaxation and filling of the LV were first described by Ling et al. [1]. They reported 2 to 5 mmHg pressure difference between the mid-left ventricle and the apex in eight dog hearts during passive filling and a 2 to 3 mmHg reversed pressure difference (apical pressure exceeds mid-ventricular pressure) during late filling. Also, in a dog heart, Courtois et al. [2] observed a significant subbasal-apical early diastolic pressure gradient along the LV inflow tract with minimum pressure in the apex speculating suction of the blood toward the LV apex.

Recently, color *M*-mode Doppler (CMD) has been introduced as a noninvasive bedside method for assessment of LV filling flow [3] and indirectly of pressure differences [4]. It provides a spatio-temporal velocity distribution $v(s, t)$ along a scanline with a typical temporal resolution of 5 ms, a spatial resolution of 300 $\mu$m, and a velocity resolution of 3 cm/s. CMD echocardiographic data can be obtained along a scanline from the left atrium, through the mitral valve, to the left ventricle. A key parameter derived from the CMD is the E-wave propagation velocity (WPV), i.e., the slope of the leading edge of the CMD derived E-wave. This propagation velocity is significantly less than the maximum velocity of the E-wave and appears to provide important independent information about left ventricular filling pressures and diastolic function [5]. It has already been shown [6,3,7] that there exists a relation between WPV and the time constant $\tau_v$ of LV isovolumetric relaxation. Garcia [8] correlated capillary wedge pressure as an index of left atrial pressure with E-wave velocity and WPV.

Vortex formation during filling is an experimentally observed phenomenon, and according to Bellhouse [9] the presence of a vortex ring provides a mechanism for early valve closure in diastole. More recently, Steen and Steen [10] showed in vitro that at the start of filling, blood moves simultaneously at all positions, behaving as an incompressible fluid column (phase I). Then they observed a flow wave propagating from the mitral orifice toward the apex (phase II). In this phase, a ring vortex was seen to travel from the orifice toward the apex. Shortland et al. [11] studied vortex formation and traveling in a skeletal muscle ventricle. They suggested that vortex traveling is an important feature to decrease cellular residence time in the apical region.

Computer models describing cardiac filling are mostly limited to the fluid dynamic process (one-dimensional lumped models based on electrical analogy, two-dimensional analytical models or two-dimensional and three-dimensional numerical models) or are meant to assess myocardial function focused on the quantification of ventricular wall stresses and deformations that occur during diastole. Peskin [12] was the first to model the fluid–ventricular wall interaction using the immersed boundary method. Owen [13] developed a one-dimensional model showing the importance of intraventricular pressure wave propagation during early filling. Redaelli et al. [14] computed the LV ejection in a two-dimensional model accounting for the local interaction between the cardiac wall and the intraventricular fluid. They were able to simulate intraventricular pressure gradients during systole. Henry et al. [15] simulated vortex propagation during ventricular filling in a skeletal muscle ventricle (SMV). In this study, the wall motion was prescribed from experiments.

The present work, by means of a two-dimensional computational approach, evaluates the fluid dynamics of filling for an axisymmetric LV. The interaction between the ventricular wall and the fluid is taken into account. The method is used to calculate flow and pressure patterns in the LV during the filling phase. The calculated flow patterns can be transformed into the format of a color Doppler *M*-mode echocardiogram. A qualitative comparison is made with measured intraventricular pressure profiles, reported

Contributed by the Bioengineering Division for publication in the JOURNAL OF BIOMECHANICAL ENGINEERING. Manuscript received by the Bioengineering Division May 18, 1999; revised manuscript received July 9, 2000. Associate Technical Editor: C. R. Ethier.

  

in the literature. The particular behavior of the intraventricular pressure curves is explained based on the results of the simulation. The long term goal of our model is to study the predictive value of noninvasive parameters (e.g., velocities measured with Doppler echocardiography) on invasive parameters (e.g., pressures, stiffness of cardiac wall, time constant of relaxation). Hereby, an important clinical question to be solved is: ''How can a stiffer ventricle be distinguished from a normal ventricle by a noninvasive technique, if no distinction can be made by the mitral velocity profile measured by pulsed Doppler echocardiography?'' [16]. We suggest that this information may be derived from color *M*-mode Doppler measurements by measuring WPV.

## Methods

**Intraventricular Blood Model.** The fluid domain of the LV is described by means of an axisymmetric model. The fluid flow is computed with a finite volume method (FVM) based on Arbitrary Lagrangian–Eulerian (ALE) formulation of the full Navier–Stokes equations. The ALE formulation allows the computation of the flowfield on a moving mesh. A triangular mesh with 1056 nodes (Fig. 1) is used to represent the axisymmetric intraventricular cavity. Details about the implementation can be found in Appendix A. The movement of the mesh is computed from the movement of the boundary with the method of Riemslagh et al. [17].

The computation is started after the onset of isovolumetric relaxation (IVR). During the IVR phase, the fluid is assumed to be quiescent inside the ventricle, i.e., velocities are zero and no pressure differences are present. In this phase, the pressure drop in all nodes is computed according to the change of Young's modulus in the ventricular wall model. When the ventricular pressure drops below the atrial pressure, the mitral valve opens. From this moment, a blunt mitral velocity profile is applied at the orifice (base) of the ventricle and the pressure at the base follows from the computation. After opening of the mitral valve, pressure in the ventricle is determined by both the relaxation of the ventricular wall and the dynamics of the blood flow. The blood is assumed to behave as a Newtonian fluid with a density of 1050 kg/m$^3$ and kinematic viscosity of $2.54\times10^{-6}$ m$^2$/s.

The mitral flow pattern that is used as boundary condition and the atrial pressure at opening of the mitral valve are derived from a separate calculation with the lumped parameter model developed by Meisner [18].

**Ventricular Wall Model.** The LV wall is described by a truncated ellipsoid in the zero stress state. At the zero stress state and with the blood at rest, the transmural pressure is zero. The zero stress state is assumed to correspond with a volume $V_0 = 12$ ml, diameter of mitral annulus of 1.5 cm, and base to apex distance of 4 cm. These are physiological parameters for a canine heart.

The discretization of the ventricular wall in this zero stress state is shown in Fig. 1. Identical nodes are used (65 nodes) to represent the position of the ventricular wall and the boundary of the fluid domain. So, no interpolation is necessary to exchange data between the wall and blood models.

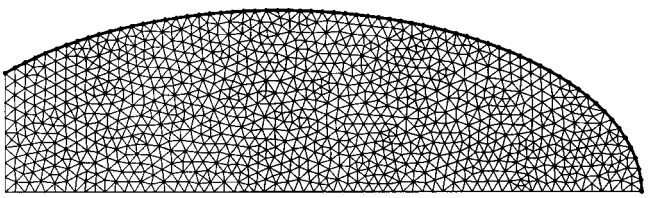

**Fig. 1 Discretization of the ventricle with corresponding boundary discretization**

Away from the zero stress state, the shape of the ventricle is computed from equilibrium equations for the ventricular wall. A nonlinear extension of the thin shell equations, inspired by the work of Janz and Grimm [19] is used as constitutive law for the heart muscle:

$$N_{\theta_i} = \frac{Eh}{\alpha(1+\nu)}\left[e^{\alpha\varepsilon_{\theta\theta_i}} - e^{-\left[\alpha\nu/(1-\nu)\right](\varepsilon_{\theta\theta_i}+\varepsilon_{\phi\phi_i})}\right],$$

$$N_{\phi_i} = \frac{Eh}{\alpha(1+\nu)}\left[e^{\alpha\varepsilon_{\phi\phi_i}} - e^{-\left[\alpha\nu/(1-\nu)\right](\varepsilon_{\theta\theta_i}+\varepsilon_{\phi\phi_i})}\right].$$

The tensions $N_{\theta_i}$ and $N_{\phi_i}$ are denoted in Fig. 9. $E$ is Young's modulus for small strains $\varepsilon_{\theta\theta_i}$ and $\varepsilon_{\phi\phi_i}$; $\alpha$ is a parameter that describes the nonlinear behavior of the heart muscle, for $\alpha$ going to zero, the linear thin shell equations are retrieved; $h$ represents the wall thickness of the ventricle in the zero stress state. With this choice, no further changes of $h$ with ventricular volume have to be taken into account. The heart wall is assumed to be incompressible, so that Poisson's coefficient $\nu$ is equal to 1/2. For each node describing the boundary, equilibrium in radial and axial direction is expressed as a function of the axial ($x$) and radial ($r$) position of the node. The mitral valve annulus is kept fixed, so the corresponding node is not allowed to move. The apical node can only move in the axial direction, so only equilibrium in axial direction is expressed for this node. The definition of the strains $\varepsilon_{\theta\theta_i}$ and $\varepsilon_{\phi\phi_i}$ and the equilibrium equations are given in Appendix B.

During relaxation, the compliance of the ventricle is changing. This is modeled by changing Young's modulus as a function of time:

$$E = E_{\text{start}} + (E_{\text{stop}} - E_{\text{start}})(1 - e^{-t/\tau_v}),$$

where $t$ denotes the time and $\tau_v$ the time constant of relaxation. $E_{\text{start}}$ is the modulus at the onset of IVR and $E_{\text{stop}}$ is the modulus in the passive state of the heart muscle. Young's modulus $E$ and the nonlinearity parameter $\alpha$ are assumed to be constant along the heart wall. $V_0$, $E_{\text{stop}}$, and $\alpha$ are determined by the fitting of a given diastolic PV relationship for the ventricle [20], $h$ and $\tau_v$ are chosen and $E_{\text{start}}$ is derived from end systolic pressure (ESP), computed with Meisner's model (see below). The values $E_{\text{start}} = 33.5$ kPa, $E_{\text{stop}} = 709$ Pa, $h = 1$ cm, $\alpha = 5.35$, and $\tau_v = 30$ ms are used.

The system of equations describing the position of the heart wall is linearized by Newton's method (derivatives are calculated numerically) and solved with a direct solver (band solver) or block Jacobi iterations.

**Coupling Procedure.** The solution on the new time level satisfies both the flow equations and the heart wall equations. To reach the global solution, an iteration procedure is used, alternating between the fluid model and the heart wall model. The boundary conditions during the solution phase of one model do not contain details of the other model.

The different steps needed to solve the different subproblems are:

1 Estimate the pressure drop due to relaxation of the heart muscle between $t$ and $t+\Delta t$. This pressure drop is applied to all nodes in the mesh.

2 Calculate a better approximation for the displacement of the heart wall with the known pressure distribution along the wall (1 block Jacobi iteration).

3 Calculate a better approximation for the position of the internal nodes with the new position of the heart wall (20 block Jacobi iterations).

4 Update the flow problem, given the inflow velocity, the displacement of the boundary and the displacement of the internal nodes, resulting in a new pressure distribution along the heart wall (1 multistage iteration).

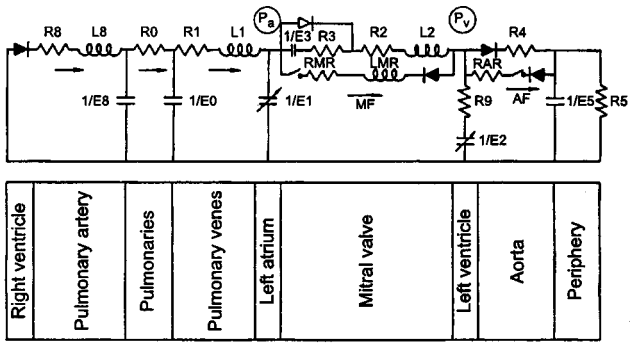


| $R$ (mmHg/(ml/s)) | $L$ (mmHg/(ml/s$^2$)) |
|---|---|
| $R_0 = 0.18$ | $L_1 = 0.002$ |
| $R_1 = 0.1$ | $L_2 = 0.002$ |
| $R_3 = 4$ | $L_8 = 0.004$ |
| $R_4 = 0.1$ | $L_{MR} = 0.002$ |
| $R_5 = 2.4$ | |
| $R_8 = 0.02$ | $E$ (mmHg/ml) |
| $R_9 = 0.00001$ | $E_0 = 0.48$ |
| $R_{MR} = 0$ | $E_3 = 1280$ |
| $R_{AR} = 0$ | $E_5 = 1.25$ |
| $R_2 = 0.0001$ mmHg/(ml/s)$^2$ | $E_8 = 0.32$ |

**Fig. 2 Electric analogy for the circulation [18]. $R_2$ is a quadratic resistance.**

5 Repeat from step 2 until convergence for all subproblems is achieved.

Note that the flow problem cannot be solved if the displacement of the cardiac wall does not correspond with the flow entering the ventricle, since the continuity equation then cannot be fulfilled. Therefore, an artificial compressibility method is used (see Appendix A) that allows an update of the flow problem; e.g., if a larger volume of fluid is entering the ventricle than the volume displaced by the boundary, pressure will rise in cells with a mass imbalance, leading to a pressure rise at the cardiac wall too. This pressure rise at the cardiac wall is used as input for the heart wall model, leading to a displacement of the cardiac wall. Finally, after convergence of both problems, the continuity equation is fulfilled everywhere in the flowfield. The artificial compressibility method is only meant to obtain convergence of the coupling method and does not influence the final result.

**Interaction With Meisner's Model.** The two-dimensional model focuses on a part of the heart cycle. Initial conditions are computed with Meisner's lumped model, which simulates the complete heart cycle. Based on electric analogy (Fig. 2), the flow is modeled by the conjunction of resistances, inductances, capacitances, diodes, and switches. Left atrial and ventricular pressures ($P_a$ and $P_v$) are dependent on variable chamber stiffness parameters. These are denoted in the figure by $E_1$ and $E_2$. The time functions that are needed to compute $P_a$ and $P_v$ are given in Appendix C.

The mitral flow profile is computed with Meisner's model for a heartbeat of 80 beats per minute and for a time constant of ventricular relaxation $\tau_v$ equal to 30 ms. The diastolic PV relationship in Meisner's model, determined by the parameters $P_{v_\infty}$, $A_v$, and $\alpha_v$ (see Table 1), is fitted on the same PV relationship [20] so it corresponds with that of our two-dimensional model.

**Table 1 Parameters for variable components in Meisner's model**

| | |
|---|---|
| $t_{as} = 350$ ms | $P_{v_\infty} = -1.66$ mmHg |
| $\Delta t_{as} = 200$ ms | $A_v = 2.36$ mmHg |
| $E_{min,la} = 1$ mmHg/ml | $\alpha_v = 0.0445$ 1/ml |
| $E_{max,la} = 2$ mmHg/ml | $\tau_v = 30$ ms |
| $V_{da,max} = 13$ ml | $t_{vc} = 500$ ms |
| $\Delta V_{da} = 2$ ml | $E_{max,lv} = 8$ mmHg/ml |
| $\Delta t_{hb} = 750$ ms | $V_{dv} = 8.8$ ml |

An end systolic volume (ESV) of 18 ml is assumed [21]. This condition was used to determine the dead volume parameter $V_{dv}$ in Meisner's model. The computed ESP, equal to 75 mmHg, determines the parameter $E_{\text{start}}$ in the two-dimensional model:

$$E_{\text{start}} = E_{\text{stop}} \frac{ESP}{P_{DPV,V=ESV}}$$

where $P_{DPV,V=ESV}$ is the pressure according to the diastolic PV relationship for a volume equal to ESV.

The mitral valve opens when the ventricular pressure becomes smaller than the atrial pressure. This happens in the calculation with Meisner's model for a ventricular pressure equal to 6.75 mmHg. When the ventricular pressure drops below this value in the two-dimensional model, the flow pattern computed from Meisner's model is applied as inflow boundary condition.

## Validation

Pressure wave propagation in a cylindrical elastic tube was computed in order to validate the present method. The length and radius of the tube are respectively 5 cm and 12 mm, which are representative values for the LV. The wall characteristics are determined by the parameter *Eh* (Appendix B). Here *Eh* was chosen to be 19.8 Pa m, which corresponds with a mean value of the heart wall during the filling phase.

The mesh used for this computation is shown in Fig. 3 and has 893 nodes, comparable with the mesh used for the LV. The time step is equal to the one for the LV computation and is 1.5 ms. The influence of viscosity is neglected for the validation.

The finite wave speed in a flow of an incompressible inviscid fluid in a cylindrical elastic tube is analytically given by the Moens–Korteweg relationship:

$$c = \sqrt{\frac{Eh}{2\rho r}},$$

where $c$ is the wave speed and $\rho$ the density of the fluid. Here, density of blood is assumed to be $\rho = 1050$ kg/m$^3$. The Moens–Korteweg wave speed with previous parameters is 0.886 m/s.

At the inlet of the tube, a velocity profile is applied with a small amplitude, compared to the wave speed, so that the Moens–

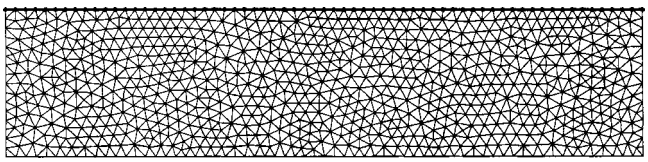

**Fig. 3 Discretization of two-dimensional axisymmetric elastic tube**

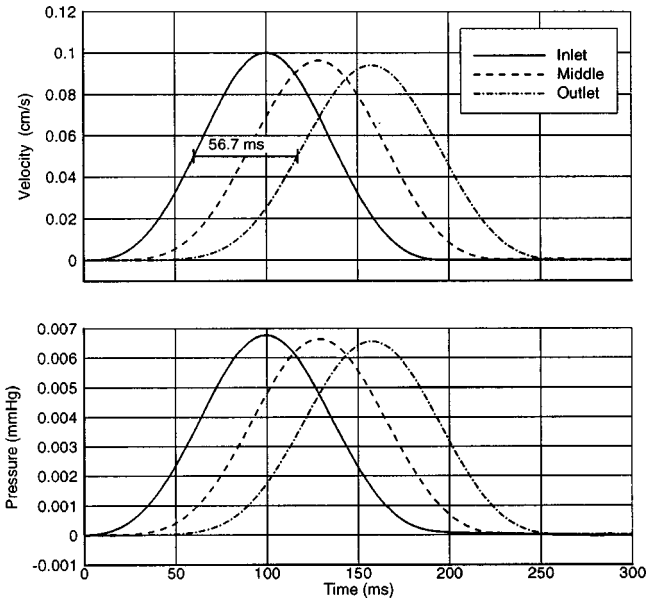


**Fig. 4 Flow calculation in two-dimensional axisymmetric elastic tube, no reflection at outlet. Velocity (top) and pressure (bottom) profiles at inlet, middle, and outlet of tube.**

Korteweg relationship is valid. This is shown in Fig. 4. The inlet profile corresponds with a fifth-order polynomial, with first and second derivatives at time 0 and 200 ms equal to zero. This period is representative for the duration of an early filling wave in the LV. At the outlet of the tube, a nonreflecting boundary condition is applied. So, no reflections can occur within the tube. The pressure wave propagation speed can then be measured from the time delay between the velocity profile at the inlet and the outlet of the tube. This time delay is 56.7 ms and the corresponding wave speed is 0.882 m/s. This is a difference of less than 1 percent with the Moens–Korteweg wave speed.

This shows that the coupling of both subproblems gives the correct physical behavior with an excellent accuracy.

## Results and Discussion

The amplitude of the mitral velocity as a function of time, computed with Meisner's model, is shown in the top part of Fig. 6. The first peak is due to ventricular relaxation and is called the early filling wave (E-wave). The second peak is due to atrial contraction and is called the A-wave. The computation ends before the ventricular contraction in Meisner's model ($t = 500$ ms). The jump in pressure at the base at the end of filling is due to the discontinuity in the velocity profile at the end of the A-wave.

Figure 5 shows velocity vectors and isobars at four time steps during filling: peak velocity during early filling (E-wave), diastasis, peak velocity during atrial contraction (A-wave), and deceleration of the A-wave. The filling is characterized by different vortex movements. A first vortex is formed before the maximum of the early filling wave occurs at the mitral annulus. The vortex is amplified during the deceleration phase of the early filling wave and moves inside the ventricle towards the apex. Between E- and A-wave (diastasis) one big vortex can be seen in the whole ventricle. At the base a second vortex can be detected, with the direction of rotation opposite to the first vortex. During the acceleration phase of the A-wave the second vortex grows, while a third vortex is formed, comparable to the first one. During the deceleration phase of the A-wave the second vortex disappears. The first vortex is now located at the apex and the third one fills the basal region. The vortex formation during filling is an experimentally observed phenomenon [10,9,22]. Shortland et al. [11]

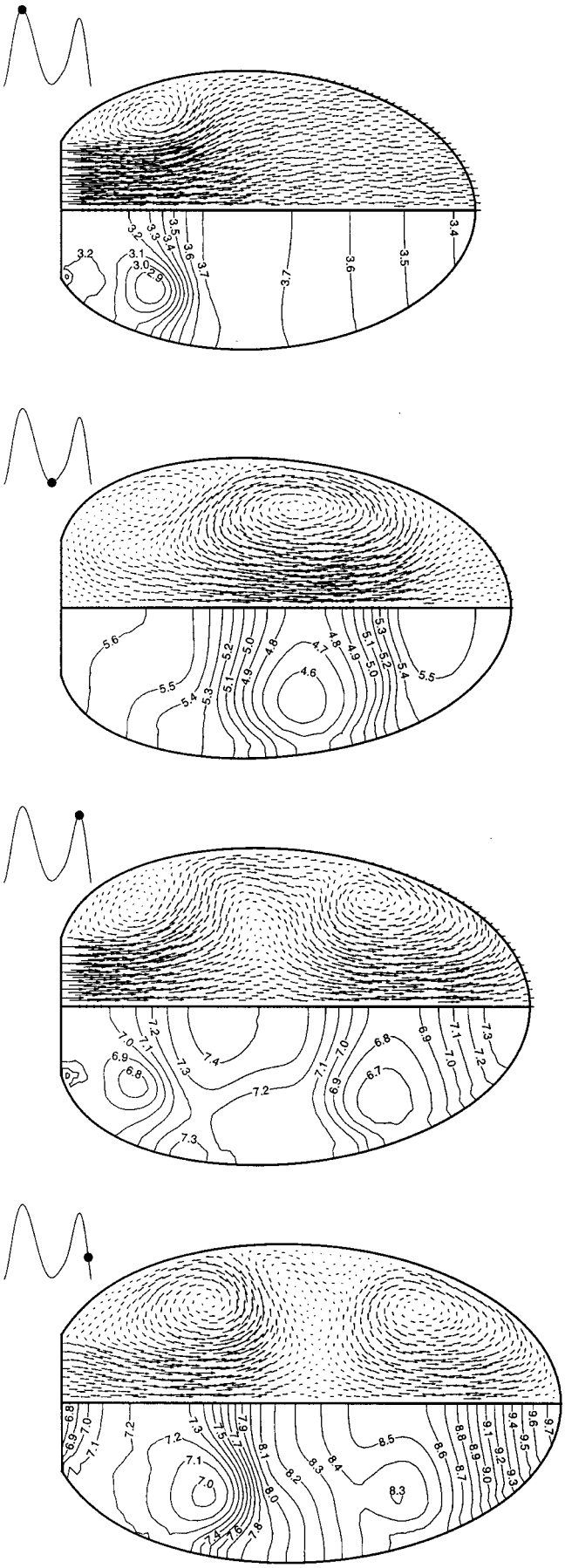

**Fig. 5 Flow patterns and isobars in the LV during filling**

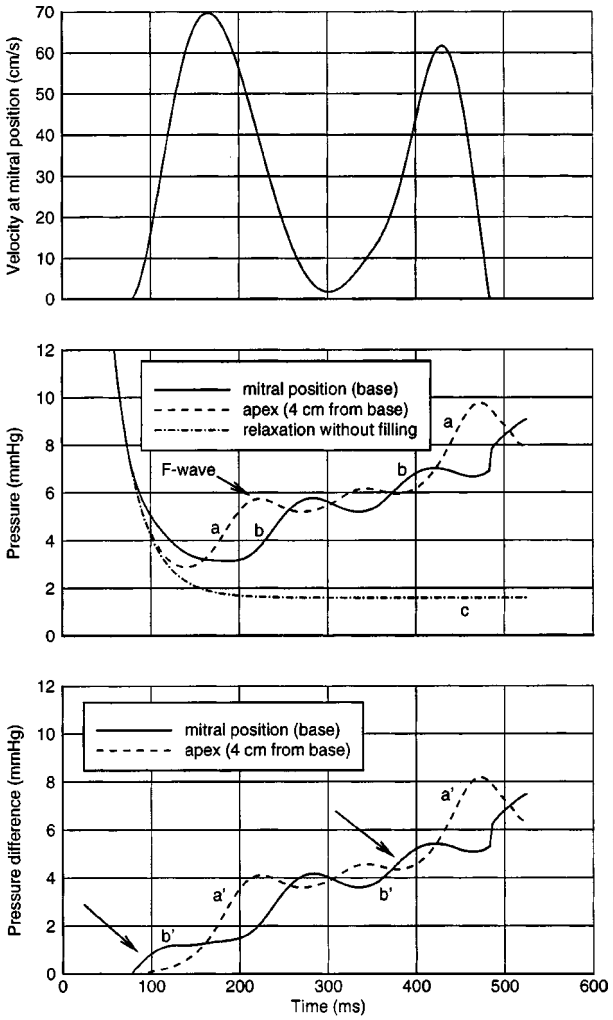


**Fig. 6 Top: Velocity profile at mitral valve. Middle: Computed pressure profiles at mitral valve (base) and apex with inflow (*a*: apex, *b*: base) and without inflow (relaxation without filling, curve *c*). Bottom: Pressure profiles at mitral valve and apex obtained by subtraction of curve *c* from curves *a* and *b* (*a′*: apex, *b′*: base). For both the E-and the A-wave, there is first a pressure rise at the base (see arrows) and then at the apex.**

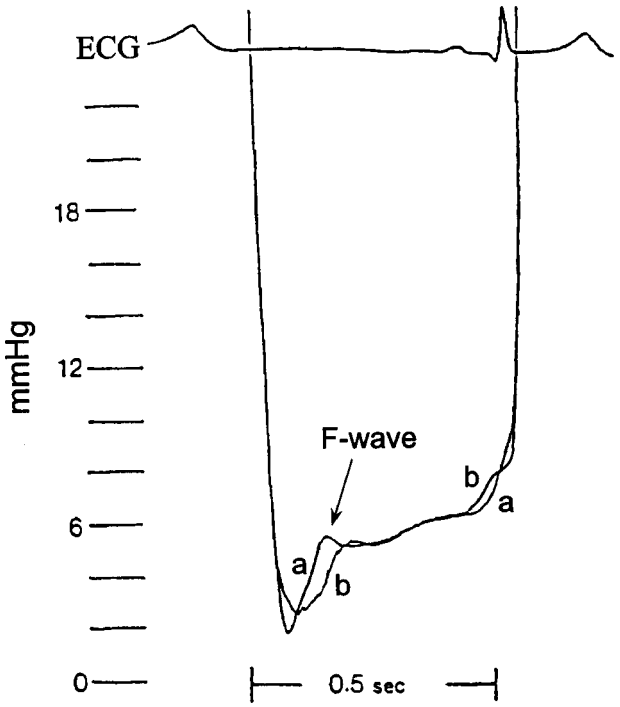


**Fig. 7 Measured intraventricular pressure waveforms [2], *a*: apex, *b*: base**

described also the formation of series of smaller secondary vortices in the wake of the primary vortex. In their experiments no A-wave was present.

Figure 6 shows calculated intraventricular pressures as a function of time. Pressures curves at base (*b*) and apex (*a*) are shown. The third curve represents the pressure in the LV if the mitral valve does not open. This curve is computed by the two-dimensional model with the same initial conditions but zero mitral velocity is applied as boundary condition. The bottom part shows the difference of the pressure curves at base and apex with and without opening of the mitral valve.

Figure 7 shows intraventricular pressures recorded by Courtois et al. [2]. Courtois observed that the smallest diastolic pressure is obtained at the apex, the pressure rise during the early filling phase occurs first at the apex, then at the base. The pressure drop at the apex is followed by a strong pressure rise, called the F-wave. During the A-wave, the pressure rises first at the base, then at the apex. Courtois stated that during systole, elastic energy is stored in the apex. At the onset of diastole, this results in an elastic recoil of the apex and a suction of blood toward the apex, leading to overfilling of the apex. Once the apex is filled, blood flows back to the midventricular and basal regions. He associated these phenomena with an active filling. The pressure rise during atrial contraction is first observed at the base and later at the apex. He concluded that this corresponds with a passive filling.

Figure 6 shows that in the simulation the smallest diastolic pressure is obtained at the apex and that the pressure rise during early filling first occurs at the apex and then at the base. The F-wave is also reproduced. At the onset of atrial contraction, there is first a pressure rise at the base and then at the apex. However, no coincidence of apical and basal pressure waveforms is present, as is the case in Fig. 7. This might be due to the absence of the long diastasis period in our simulation.

The physiological phenomena are reproduced in the computer simulation. However, elastic energy was not stored in the model, which means that Courtois' hypothesis cannot be the explanation for the behavior of the observed pressure curves. Figure 6 shows that if the mitral valve does not open, the pressure in the ventricle would further drop due to relaxation (curve *c*). If the valve opens, the pressure at the base deviates from curve *c*. This corresponds to the start of a pressure wave, which originates at the base and moves in the direction of the apex. We call this wave the pressure filling wave. By comparing the pressures at the mitral and the apex positions immediately after the onset of the wave (Fig. 6), we see that the pressure gradient in the direction of the wave propagation is negative, so it is a compression wave. However, the pressure does not rise if the wave passes by, because the relaxation is still going on. The actual pressure is formed by a superposition of a pressure drop due to relaxation and a pressure rise due to the compression. Initially, the influence of the relaxation on the pressure profile is much stronger. The pressure at the apex follows curve *c* much longer, indicating that the pressure filling wave has not reached the apex yet. When the wave reaches the apex, it is reflected at the apex as a second compression wave in the the direction of the base (reflection at a closed end). This reflection of the pressure wave at the apex was already described by Owen [13]. The pressure rise exceeds the pressure drop due to relaxation, which causes the minimum in the pressure profile. Due to the reflection at the apex, the pressure rise is about twice as

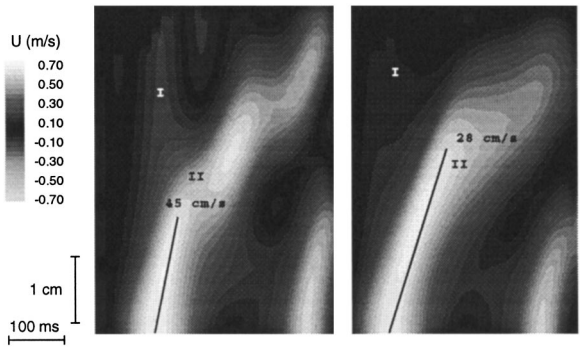


**Fig. 8 Color *M*-mode echocardiogram (here grayscale) derived from a two-dimensional axisymmetric flow simulation. Along the horizontal axis the time evolution is shown. The vertical axis represents the distance in the ventricle along the centerline. The bottom corresponds with the base and the top with the apex. Velocities along the symmetry axis are color coded. Both the early and atrial filling wave can be seen, the initial flow phase with blood moving simultaneously in the ventricle is denoted as I, the propagation of the early filling wave is denoted as II. Left: reference calculation. Right: calculation with same mitral inflow pattern, but higher LV stiffness ($E_{stop}$=8.85 kPa) and thus higher atrial pressure at opening of the mitral valve (25 mmHg).**

strong than at the base, which results in the F-wave in Fig. 6. The described phenomena show that the filling is of passive type.

This can be seen more clearly in the bottom part of Fig. 6, where curve *c* is subtracted from curves *a* and *b*. In this way, the influence of homogeneous relaxation on the pressure profile is eliminated. For both the E- and the A-waves, there is first a pressure rise at the base (see arrows) and then at the apex, showing that both are passive filling waves. In the previous explanation, we omitted the influence of the pressure rise due to the enlargement of the ventricular volume during filling (static diastolic PV relationship). This explains why the curves in the bottom part of Fig. 6 are still rising.

That filling starts at the base can also be seen in a color *M*-mode Doppler (CMD) echocardiogram. The CMD shows time evolution along its horizontal axis, depth information along its vertical axis, and velocity information by color coding. Figure 8 shows a CMD along the symmetry axis, calculated with the present model.

Both the early (E) and atrial (A) filling waves can be seen. During the initial flow phase, blood moves almost simultaneously in the whole ventricle, which can also be seen in the top part of Fig. 5. This phase is denoted as I in Fig. 8. The movement is caused by the passing of the pressure filling wave. The filling causes the generation of a vortex, as described earlier. The propagation of this vortex determines the propagation of the maximum velocity along the symmetry axis of the LV as can be seen in Fig. 5. The propagation of the maximum velocity is seen in the CMD and is denoted as phase II in Fig. 8. We call this vortex propagation the flow filling wave. The flow wave propagation velocity (WPV) is determined by measuring the slope of the CMD pattern, as shown in Fig. 8. Both phases (I and II) were experimentally observed by Steen and Steen [10].

For the reference calculation shown in the left panel, the maximal blood velocity at the mitral valve during early filling is 70 cm/s and the WPV is 45 cm/s. The ratio is 1.56. This hemodynamic behavior was also observed in experiments in vitro [1] and in measurements in vivo [2].

The right panel shows the CMD of a calculation with higher LV stiffness ($E_{stop}$=8.85 kPa). The initial conditions and the mitral inflow pattern are the same as for the reference calculation. The atrial pressure at opening of the valve is raised to 25 mmHg. Otherwise no filling occurs. This increased preload condition simulates a diseased state. The WPV decreases from 45 to 28 cm/s. This result may indicate that there exists an inverse relationship between WPV and LV stiffness, suggesting that WPV is an important noninvasive parameter to assess directly LV diastolic stiffness and indirectly LV diastolic pressure and atrial pressure, since higher diastolic stiffness leads to higher diastolic pressure (through the PV relationship) and thus higher atrial pressure (preload) to maintain adequate filling.

## Limitations of the Model

A simple model for the cardiac muscle is used. Stress distributions in radial direction are lumped because the model only has to provide pressure as a function of the position of the endocardial wall surface. Regional differences in Young's modulus *E*, nonlinearity parameter $\alpha$, and thickness *h* are not taken into account for simplicity. Elastic recoil and diastolic suction [23] are not modeled since no bending moments are introduced in the cardiac wall model. This is not necessary, because in our computation there is no influence of elastic recoil present since ESV is larger than the zero stress volume. The influence of the papillary muscles and the LV twist during relaxation are neglected. Their impact should be investigated in the future. The model is two-dimensional axisymmetric. Therefore, the influence of real three-dimensional effects, such as the orientation of the mitral valve, cannot be studied. Iudicello [24] showed that the vortex becomes asymmetric when an offset angle at the entrance to the ventricle is present. This can alter the WPV.

During the filling phase it is assumed that forces of the mitral valve on the fluid are small. Therefore, the valve is not modeled. Also inertial forces of the heart wall are neglected. The first phase of the calculation is the IVR. It is assumed that initially the flow is at rest and that IVR is homogeneous. Then there is no blood movement during relaxation and intraventricular pressure gradients are absent. In vivo, IVPGs can occur during this phase [25], but these are small compared with IVPGs during systole or diastole.

## Conclusions

A two-dimensional axisymmetric computer model for the LV filling flow was developed. The pressure curves obtained correspond well with measured pressure curves reported in the literature. The specific form of the pressure curves can be explained as a result of superposition of the pressure drop in the ventricle due to relaxation and the passive filling wave (compression wave) starting at the base toward the apex. This explanation differs from Courtois' interpretation [2] where the particular form of the pressure curves was seen as evidence of elastic recoil of the LV. Our interpretation does not exclude the presence of elastic recoil during the early filling phase. However, elastic recoil does not cause the particular pressure profiles. The vortex formation during filling as observed by Bellhouse [9], Lee and Talbot [22], Steen and Steen [10], and Shortland et al. [11] is reproduced in the simulation. From a calculated color Doppler *M*-mode echocardiogram, it can be seen that both the early and atrial filling waves travel from base to apex. Blood velocities are higher than the WPV, which corresponds with in vitro measurements by Steen and Steen [10] and in vivo measurements by Stugaard et al. [6]. Higher LV stiffness results in a smaller WPV for a given peak E velocity. This result may indicate an inverse relationship between WPV and LV stiffness, suggesting that WPV may be an important noninvasive index to assess LV diastolic stiffness, LV diastolic pressure, and thus atrial pressure (preload).

## Acknowledgments

The research reported here was granted by contract GOA-95003 of the concerted action program of the Ghent University, supported by the Flemish government.

## Appendix A: The Flow Model

**Flow in Moving Domain.** For a moving control volume, the equations of conservation of mass and conservation of momentum are given by the ALE formulation of the Navier–Stokes equations:

$$\frac{\partial}{\partial t}\int_V \rho dV + \int_S \rho(\underline{v}-\underline{v}_b)\cdot\underline{n}dS = 0, \tag{1}$$

$$\frac{\partial}{\partial t}\int_V \rho\underline{v}dV + \int_S (\rho\underline{v}(\underline{v}-\underline{v}_b)+p\underline{\underline{I}}-\underline{\underline{\tau}})\cdot\underline{n}dS = 0. \tag{2}$$

Here $\rho$ is the density, $\underline{v}$ the velocity vector of the fluid in a fixed coordinate system, $\underline{v}_b$ the velocity vector of the boundary $S$ of the control volume $V$, $\underline{n}$ the normal external to this boundary, $\partial/\partial t$ the time derivative, $p$ the pressure, $\underline{\underline{I}}$ the unit tensor, $\underline{\underline{\tau}}$ the viscous-stress tensor defined for a Newtonian fluid by $\underline{\underline{\tau}}=2\mu\underline{\underline{\gamma}}$ with $\underline{\underline{\gamma}}$ the rate-of-strain tensor $\gamma_{i,j}=(1/2)(\partial v_i/\partial x_j+\partial v_j/\partial x_i)$ and $\mu$ the dynamic viscosity.

The velocities $\underline{v}_b$ have to satisfy the space conservation law

$$\frac{\partial}{\partial t}\int_V dV - \int_S \underline{v}_b\cdot\underline{n}dS = 0.$$

When constant density is assumed, Eq. (1) can be written as

$$\int_S \underline{v}\cdot\underline{n}dS = 0.$$

We discretized this form of the continuity equation together with the momentum Eq. (2). At the inlet, the velocity is prescribed, along the cardiac wall, the displacement is prescribed, and along the axis of symmetry, velocity is zero. The pressure at the boundaries is extrapolated from the flow field with

$$\underline{n}\cdot\left(\rho\frac{D\underline{v}}{Dt}\right) = -\underline{n}\cdot\nabla p = -\frac{\partial p}{\partial n}$$

where $D$ stands for the material derivative and $n$ is the unit vector in the direction normal to the boundary.

**Discretization.** The discretization of the Navier–Stokes equations is done on an unstructured triangular mesh. The nodes are connected by Delaunay triangulation. A central discretization is used for the acoustic part, i.e. the velocities in the continuity equation and the pressure in the momentum equations. The viscous terms are also discretized with a central scheme. The convective part in the momentum equations is discretized using velocity upwinding. Since the pressure terms are discretized centrally, an artificial dissipation term in pressure is added to the continuity equation [26]. The discretization is written on a 2D axisymmetric mesh. The time integration is performed with the one-step implicit backward Euler method.

**Iteration Method.** The discrete system can be written as:

$$\frac{1}{\Delta t}V_i^{n+1}W_i^{n+1} + P_{i,0}^{n+1}Q_i^{n+1} + \sum_k P_{i,k}^{n+1}Q_k^{n+1} + R_i^{n+1} = \frac{1}{\Delta t}V_i^n W_i^n .$$

where $Q=\{p, u, v\}^T$ and $W=\{0, u, v\}^T$. The sum is taken over all the neighboring nodes $k$ of node $i$. The coefficient matrices $P$ have $3\times3$ components and contain contributions from the acoustic discretization, the pressure stabilization, and the viscous discretization. The discretizations of these linear parts of the equation remain linear. The vector $R_i$ collects the convective first and second order terms.

This system is solved with a multistage pseudo-time-stepping method. A standard four-stage scheme is used with coefficients {1/4, 1/3, 1/2, 1}. The update $\Delta Q^m = Q^{m+1}-Q^m$ used in each stage of the multistage is derived from

$$\Gamma\frac{1}{\Delta\tau}V_i^m\Delta Q_i^m + \frac{1}{\Delta t}V_i^m W_i^{m+1} + P_{i,0}^m Q_i^{m+1} + \sum_k P_{i,k}^m Q_k^m + R_i^m = \frac{1}{\Delta t}V_i^n W_i^n ,$$

where $m$ indicates the iteration level in the multistaging. In pseudo-time $\tau$ a preconditioning matrix is used given by $\Gamma=\mathrm{diag}\{1/\beta^2,1,1\}$ where $\beta$ is a pseudo-compressibility coefficient, equal to the local velocity and prohibited from becoming zero. Convergence is obtained for each time step if $\Delta Q_i^m=0$. So, there is only influence of the artificial compressibility during the iteration process, not in the solution of each time step.

## Appendix B: Heart Wall Model

**Definition of Strains.** For the control volume in Fig. 9, the circumferential strain $\varepsilon_{\theta\theta_i}$ is given by

$$\varepsilon_{\theta\theta_i} = \frac{2\pi r_i - 2\pi r_{0_i}}{2\pi r_{0_i}}.$$

The meridional strain between node $i$ and $i+1$ is given by

$$\varepsilon_{\phi\phi_{i+1/2}} = \frac{l_{i+1/2}-l_{0_{i+1/2}}}{l_{0_{i+1/2}}},$$

with

$$l_{i+1/2} = \sqrt{(x_{i+1}-x_i)^2+(r_{i+1-r_i})^2},$$

the distance between node $i$ and $i+1$. The index $_0$ denotes the zero stress state.

**Equilibrium Equations.** For small $d\theta$, the equilibrium in axial direction is given by

$$N_{\phi_{i+1/2}}\cos\phi_{i+1/2}r_{i+1/2}d\theta - N_{\phi_{i-1/2}}\cos\phi_{i-1/2}r_{i-1/2}d\theta - p_i\frac{d\theta}{2}(r_{i+1/2}^2-r_{i-1/2}^2)=0.$$

The equation can be divided by $d\theta$ so that it becomes independent of $d\theta$. $\phi$ is the angle between the meridian and the axis of symmetry as denoted in Fig. 9. The radius $r_{i+1/2}$ is the mean of radii $r_i$ and $r_{i+1}$. $r_{i-1/2}$ is computed in a similar way.

Again for small $d\theta$, the equilibrium in radial direction is given by

$$N_{\phi_{i+1/2}}\sin\phi_{i+1/2}r_{i+1/2}d\theta - N_{\phi_{i-1/2}}\sin\phi_{i-1/2}r_{i-1/2}d\theta - 2N_{\theta_i}l_i\sin(d\theta/2) + p_i\Delta x_i r_i d\theta = 0. \tag{3}$$

Here, $l_i=(1/2)(l_{i-1/2}+l_{i+1/2})$ and $\Delta x_i = x_{i+1/2}-x_{i-1/2}$, where $x_{i-1/2}$ and $x_{i+1/2}$ are defined in the same way as $r_{i-1/2}$ and $r_{i+1/2}$. With $\sin(d\theta/2)\approx d\theta/2$ for small $d\theta$, and after dividing by $d\theta$ the equilibrium Eq. (3) can be rewritten as

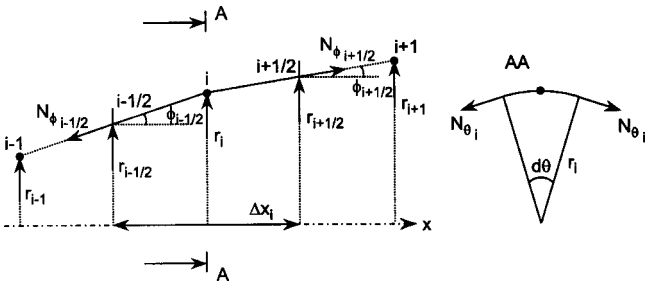


**Fig. 9 Control volume for heart wall**

$$N_{\phi_{i+1/2}} \sin \phi_{i+1/2} r_{i+1/2} - N_{\phi_{i-1/2}} \sin \phi_{i-1/2} r_{i-1/2} - N_{\theta_i} l_i + p_i \Delta x_i r_i = 0.$$

Again, the equation is independent of $d\theta$.

## Appendix C: Meisner's Model

**Left Atrium.** The relationship between left atrial pressure $P_a$ and volume $V_a$ is given by

$$P_a(t) = E_1(t)(V_a(t) - V_{da}(t)),$$

with $E_1$ a variable stiffness and $V_{da}$ a variable dead volume (volume that corresponds with zero pressure). With $t_{as}$ the start time and $\Delta t_{as}$ the duration of atrial systole, $V_{da}(t)$ and $E_1(t)$ are given by

$t \leq t_{as}$

$$V_{da}(t) = V_{da,\max}$$

$$E_1(t) = E_{\min,la}$$

$t_{as} < t \leq t_{as} + \Delta t_{as}$

$$V_{da}(t) = V_{da,\max} - \Delta V_{da} \sin\left( \pi \frac{t - t_{as}}{\Delta t_{as}} \right)$$

$$E_1(t) = E_{\min,la} + \frac{E_{\max,la} - E_{\min,la}}{2} \left( 1 - \cos\left( 2\pi \frac{t - t_{as}}{\Delta t_{as}} \right) \right)$$

$t > t_{as} + \Delta t_{as}$

$$V_{da}(t) = V_{da,\max}$$

$$E_1(t) = E_{\min,la}$$

The parameters $t_{as}$, $\Delta t_{as}$, $E_{\min,\,la}$, $E_{\max,\,la}$, $V_{da,\,\max}$, and $\Delta V_{da}$ are given in Table 1.

**Left Ventricle.** Left ventricular pressure $P_v$ and volume $V_v$ are related by

$$P_v(t) = P_{v_\infty} + A_v(e^{\alpha_v V_v(t)} - 1) + R_9 Q_m + E_2(t)(V_v(t) - V_{dv}),$$

where $P_{v_\infty}$, $A_v$, and $\alpha_v$ are parameters describing the passive LV state, $R_9$ is the resistance of the LV, $Q_m$ the mitral flow, $E_2$ a variable stiffness, and $V_{dv}$ the dead volume of the ventricle. With $\tau_v$ the time constant of ventricular relaxation, $t_{vc}$ the start time of ventricular contraction and $\Delta t_{hb}$ the duration of one heartbeat, $E_2(t)$ is given by

$t \leq t_{vc}$

$$E_2(t) = E_{\max,lv} e^{-t/\tau_v}$$

$t > t_{vc}$

$$E_2(t) = \frac{E_{\max,lv}}{2} \left( 1 - \cos\left( \pi \frac{t - t_{vc}}{\Delta t_{hb} - t_{vc}} \right) \right).$$

The end of ventricular contraction and the onset of ventricular relaxation correspond with $t = 0$. The parameters $P_{v_\infty}$, $A_v$, $\alpha_v$, $\tau_v$, $t_{vc}$, $E_{\max,lv}$, $V_{dv}$, and $\Delta t_{hb}$ are given in Table 1.

## References


[1] Ling, D., Rankin, J. S., Edwards, C. H., McHale, P. A., and Anderson, R. W., 1979, ''Regional Diastolic Mechanics of the Left Ventricle in the Conscious Dog,'' Am. J. Physiol., **236**, pp. 323–330.

[2] Courtois, M., Kovács, Jr., S. J., and Ludbrook, P. A., 1988, ''Transmitral Pressure-Flow Velocity Relation: Importance of Regional Pressure Gradients in the Left Ventricle During Diastole,'' Circulation, **78**, pp. 661–671.

[3] Brun, P., Tribouilloy, C., Duval, A. M., Iseriu, L., Meguira, A., Pelle, G., and Dubois-Randé, J. L., 1992, ''Left Ventricular Flow Propagation During Early Filling Is Related to Wall Relaxation: a Color *M*-Mode Doppler Analysis,'' J. Am. Coll. Cardiol., **20**, pp. 420–432.

[4] Greenberg, N. L., Vandervoort, P. M., and Thomas, J. D., 1996, ''Instantaneous Diastolic Transmitral Pressure Differences From Color Doppler *M*-Mode Echocardiography,'' Am. J. Physiol., **271** (Heart. Circ Physiol. **40**), pp. H1267–H1276.

[5] Thomas, J. D., Garcia, M. J., and Greenberg, N. L., 1997, ''Application of Color Doppler *M*-Mode Echocardiography in the Assessment of Ventricular Diastolic Function: Potential for Quantitative Analysis,'' Heart Vessels, **12**, pp. 135–137.

[6] Stugaard, M., Risöe, C., Halfdan, I., and Smiseth, O. A., 1994, ''Intracavitary Filling Pattern in the Failing Left Ventricle Assessed by Color *M*-Mode Doppler Echocardiography,'' J. Am. Coll. Cardiol., **24**, pp. 663–670.

[7] Takatsjuji, H., Mikami, T., Urasawa, K., Teranishi, J.-I., Onozuka, H., Takagi, C., Makita, Y., Matsuo, H., Kusuoka, H., and Kitabatake, A., 1996, ''A New Approach for Evaluation of Left Ventricular Diastolic Function: Spatial and Temporal Analysis of Ventricular Filling Flow Propagation by Color *M*-Mode Doppler Echocardiography,'' J. Am. Coll. Cardiol., **27**, pp. 365–371.

[8] Garcia, M. J., Ares, M. A., Asher, C., Rodriguez, L., Vandervoort, P., and Thomas, J. D., 1997, ''An Index of Early Left Ventricular Filling That Combined With Pulsed Doppler Peak E Velocity May Estimate Capillary Wedge Pressure,'' J. Am. Coll. Cardiol., **29**, pp. 448–454.

[9] Bellhouse, B. J., 1972, ''Fluid Mechanics of a Model Mitral Valve and Left Ventricle,'' Cardiovasc. Res., **6**, pp. 199–210.

[10] Steen, T., and Steen, S., 1994, ''Filling of a Model Left Ventricle Studied by Colour *M*-Mode Doppler,'' Cardiovasc. Res., **28**, pp. 1821–1827.

[11] Shortland, A. P., Black, R. A., Jarvis, J. C., Henry, F. S., Iudicello, F., Collins, M. W., and Salmons, S., 1996, ''Formation and Travel of Vortices in Model Ventricles: Application to the Design of Skeletal Muscle Ventricles,'' J. Biomech., **29**, pp. 503–511.

[12] Peskin, C. S., and McQueen, D. M., 1989, ''A Three-Dimensional Computational Method for Blood Flow in the Heart—I. Immersed Elastic Fibers in a Viscous Incompressible Fluid,'' J. Comput. Phys., **81**, pp. 372–405.

[13] Owen, A., 1993, ''A Numerical Model of Early Diastolic Filling: Importance of Intraventricular Pressure Wave Propagation,'' Cardiovasc. Res., **27**, pp. 255–261.

[14] Redaelli, A., and Montevecchi, F. M., 1996, ''Computational Evaluation of Intraventricular Pressure Gradients Based on a Fluid-Structure Approach,'' ASME J. Biomech. Eng., **118**, pp. 529–537.

[15] Henry, F. S., Shortland, A. P., Iudicello, F., Black, R. A., Jarvis, J. C., Collins, M. W., and Salmons, S., 1997, ''Flow in a Simple Model Skeletal Muscle Ventricle: Comparison Between Numerical and Physical Simulations,'' ASME J. Biomech. Eng., **119**, pp. 13–19.

[16] Nishimura, R. A., and Tajik, A. J., 1997, ''Evaluation of Diastolic Filling of Left Ventricle in Health and Disease: Doppler Echocardiography Is the Clinician's Rosetta Stone,'' J. Am. Coll. Cardiol., **30**, pp. 8–18.

[17] Riemslagh, K., Vierendeels, J., and Dick, E., 1998, ''Two-Dimensional Incompressible Navier–Stokes Calculations in Complex-Shaped Moving Domain,'' J. Eng. Math., **34**, pp. 57–73.

[18] Meisner, J., 1986, ''Left Atrial Role in Left Ventricular Filling: Dog and Computer Studies,'' Ph.D. thesis, Albert Einstein College of Medicine, Yeshiva University, New York.

[19] Janz, R. F., and Grimm, A. F., 1973, ''Deformation of the Diastolic Left Ventricle—I. Nonlinear Elastic Effects,'' Biophys. J., **13**, pp. 689–704.

[20] Mirsky, I., 1973, ''Ventricular and Arterial Wall Stresses Based on Large Deformation Analyses,'' Biophys. J., **13**, pp. 1141–1159.

[21] Sagawa, K., Maughan, L., Suga, H., and Sunagawa, K., 1988, *Cardiac Contraction and the Pressure–Volume Relationship*, Oxford University Press, New York.

[22] Lee, C. S. F., and Talbot, L., 1979, ''A Fluid Mechanical Study of the Closure of Heart Valves,'' J. Fluid Mech., **91**, pp. 41–63.

[23] Ingels, Jr., N. B., Daughters, G. T., Nikolic, S. D., DeAnda, A., Moon, M. R., Bolger, A. F., Komeda, M., Derby, G. C., Yellin, E. L., and Miller, D. C., 1996, ''Left Ventricular Diastolic Suction With Zero Left Atrial Pressure in Open-Chest Dogs,'' Am. J. Physiol., **270** (Heart Circ. Physiol., **39**), pp. H1217–H1224.

[24] Iudicello, F., Henry, F. S., Collins, M. W., Salmons, S., Sarti, A., and Lamberti, C., 1997, ''Comparison of Haemodynamic Structures Between a Skeletal Muscle Ventricle and the Human Left Ventricle,'' Internal Medicine, **5**, pp. 1–10.

[25] Nikolic, S., Fenely, M., Pajaro, O., Rankin, J. S., and Yellin, E., 1995, ''Origin of Regional Pressure Gradients in the Left Ventricle During Early Diastole,'' Am. J. Physiol., **268**, pp. 550–557.

[26] Vierendeels, J., Riemslagh, K., and Dick, E., 1999, ''A Multigrid Semi-Implicit Line-Method for Viscous Incompressible and Low-Mach-Number Flows on High Aspect Ratio Grids,'' J. Comput. Phys., **154**, pp. 310–341.